Experimental study on a heat driven refrigeration system based on combined organic Rankine and vapour compression cycles

Youcai Liang[1,2], Andrew Mckeow[1], Zhibin Yu[1], Saif Fraih K Alshammari[1]*

[1] James Watt School of Engineering, University of Glasgow, Glasgow G12 8QQ, UK

[2] School of Electric Power, South China University of Technology, Guangzhou, Guangdong 510640, China

* Corresponding author. Email: Zhibin.Yu@glasgow.ac.uk; Tel. +44 (0) 141 330 2530

Abstract

Waste heat recovery has been considered as an attractive technique to improve the overall energy utilization efficiency of internal combustion (IC) engines. In this paper, as distinct from most past research work, a thermally driven refrigeration system based on combined organic Rankine and vapour compression cycles is proposed to recover the IC engines' waste heat contained in the cooling water. Based on the proposed concept, a lab-scale prototype has been designed and constructed using off-the-shelf components to prove the feasibility of producing refrigeration for ships and refrigerated lorries. In this prototype, the power generated by the Organic Rankine cycle (ORC) is used to drive the compressor of a Vapour Compression Cycle (VCC) through a belt transmission mechanism. Pentafluoropropane (R245fa) and Tetrafluoroethane (R134a) are used as the working fluids for ORC and VCC systems, respectively. An electrical water heater is used to simulate the cooling jacket, while a cooling enclosure is used to simulate the cooling load. With the hot water at a temperature around 95 °C, the system

produces around 1.8 kW refrigeration effect at -4 °C, leading to an overall heat-to-cooling efficiency of 0.18, which is defined as the ratio of the cooling capacity of the refrigerator to the heat input to the ORC power plant. The system performance could be significantly improved if optimal components could be utilized.

Key words: **Organic Rankine Cycle, Vapour Compression Cycle, Waste Heat Recovery, Transport Sector, Transient**

Nomenclature		*m*	Mass flow rate (kg/s)
COP	Coefficient of Performance	*Q*	Heat (kW)
ORC	Organic Rankine Cycle	*W*	Power (kW)
VCC	Vapour Compression Cycle	*η*	Efficiency
TEV	Thermostatic Expansion Valve	***P***	pressure
SR	Speed Ratio	**Subscript**	
IC	Internal Combustion	*Cond*	Condenser
Gt	Gigaton	*Exp*	Expander
GHG	Greenhouse gas	*Com*	Compressor
PID	Proportional-Integral-Derivative	*Eva*	Evaporator
PCI	Peripheral components Interconnect	*c*	Cooling
EEV	Electronic expansion valve	*f*	Fluid
Symbols		*p*	Circulation pump
h	Specific enthalpy (kJ/kg)	*H-C*	heat-to-cooling

Introduction

Global CO_2 emissions in 2019 still remains at a high level (around 33 Gt) in spite of the rapid increase of renewable power production (mainly wind and photovoltaic) and fuel switching from coal to natural gas [1]. In the UK, transport is the largest contributor to its domestic greenhouse gas (GHG) emissions, contributing 28% of its domestic emissions in 2018 [2]. The decarbonisation of the world's economy to mitigate the impact of climate change will require us to substantially decarbonise the transport sector.

In most IC engines, around 50-65% of the thermal energy produced by burning fossil fuel is eventually discharged to the environment as waste heat through the engines' jacket water and exhaust gas. Roughly, half of the waste heat is carried away by exhaust gases, and the other half is taken away by cooling water running through the cooling jacket [3]. Therefore, it is important to improve the thermal efficiency of engines by means of waste heat recovery, which is considered to be the most promising way to improve the IC engine performance in the next 30 years.

Energy recovery from engine waste heat has attracted considerable academic and industrial research efforts. However, the recovered heat from exhaust gas is normally converted to electricity via different technologies such as thermoelectric generator and organic Rankine cycle power plants and less attention has been paid to the other types of useful output, such as cooling. For vessels, particular fishing boats, refrigeration plants are important auxiliary systems to provide air-conditioning, ice-making, and medicine or food preservation [4], typically powered by separate on board engines or

58 generators. Considering the large quantity of waste heat discharged by IC engines and
59 the vessels demand for cooling, waste heat driven cooling technologies potentially offer
60 an alternative solution.

61 There are a variety of thermally powered refrigeration technologies including
62 absorption [5,6], adsorption [7], and combined Organic Rankine cycle – Vapour
63 Compression Cycle (ORC-VCC) systems [8]. Absorption refrigeration plants have
64 been widely studied and applied to industry and district cooling networks, showing
65 remarkable energy saving benefits [9-11]. However, absorption chillers are generally
66 used for large-scale stationary applications, due to their higher complexity and large
67 space requirement. Moreover, the coefficient of performance (COP) is generally low
68 for single-stage absorption cycle systems (COP<0.7) using LiBr-H_2O pair and even
69 lower for systems using ammonia-water (NH_3-H_2O) as working fluids [12]. Adsorption
70 heat pumps or refrigerators are still at the earlier stage of lab development, and they are
71 unsuitable for mobile applications.

72 On the other hand, some effort has been devoted to the integration of ORC power
73 plant waste heat recovery system with vapour compression refrigeration systems to
74 develop a new type of heat driven cooling technology. The concept of combining ORC
75 with VCC was proposed as an alternative refrigeration method by Prigmore and Barber
76 [13]. The ORC-VCC combined cycle system is an alternative to the absorption cooling
77 cycle, which can provide either cooling or electricity when cooling is not required,
78 increasing the operational flexibility and improving the economic profitability [14,15].

79 Wali [16,17] compared the performance of solar powered ORC-VCC systems for

building cooling applications with five different working fluids. Liang [18] numerically compared two different layouts of ORC-VCC, one of which uses a belt transmission unit and the other is directly coupled using a common drive. Although directly driven units are more compact and reliable, the belt transmission unit results in a better performance since it enables the ORC-VCC to independently operate at their optimal conditions. To study the transient performance of such a concept, Kutlu et al. theoretically investigated a solar powered ORC-VCC system by considering the off-design behaviour of the system as a result of natural transient nature of solar energy [19].

To simplify the system structure for downsizing, Aphornratana and Sriveerakul [20] proposed a novel ORC-VCC concept, of which the compressor and expander are integrated in the same unit, using the same working fluid and sharing the same condenser. Bu et al. [21-23] carried out a series of investigations on the working fluid of ORC-VCC ice makers and found that n-butane (R600) is the most suitable working fluid. Based on such a system with simple structures and convenient maintenance, Bao [24] carried out performance comparison between using single fluid and dual fluid and concluded the best option for different conditions.

In addition to the above studies, several other researchers [25-28] also reported the performance of the ORC driven VCC for heating purposes. In our previous study [29], a novel ORC-VCC was proposed for heating purposes. Different from the other systems, the water is heated in two stages, firstly in the VCC condenser at a lower temperature and then in the ORC condenser at a higher temperature. The integration of ORC with

VCC in this way enables the utilisation of the low-temperature condensation heat of the vapour compression cycle.

Although there are numerous theoretical investigations on the combined ORC with VCC systems, the system performance was evaluated based some assumption, including fixed efficiency of components, fixed losses and steady conditions. However, the operation of such combined systems will be significantly affected by many factors during the practical operation, some of which can't be ignored or can't be given as fixed value. Therefore, prototyping and experimental research are very important to verify the theory and modelling. A comprehensive literature review shows that the experimental research is scarce, and only one experimental study on the ORC-VCC system was carried out by Wang [14]. Their ORC expander and the VCC compressor shared a common drive shaft to reduce energy conversion losses. However, the rotation speed and torque of the VCC compressor are exactly the same as that of the ORC expander. Meaning that the ORC and VCC can't be operated at their own optimal conditions simultaneously because the ORC's optimal condition is decided by the heat source and the VCC's optimal condition is decided by the refrigeration requirement.

In the present paper, a lab-scale prototype of the proposed ORC and VCC system has been designed and constructed using off-the-shelf components, based on which a comprehensive experimental evaluation was carried out to determine the feasibility of producing refrigeration to meet the cooling/refrigeration requirements for shipping by heat recovery of the engine's jacket water. Different from Wang's study[14], a belt transmission unit is used in the present study to change the rotational speed ratio

between ORC and VCC to find out the optimal way to connect the expander and compressor as their torque profiles differ each other. Furthermore, the prototype has been tested under both steady state and transient state conditions to understand its dynamic operational characteristics.

2 Experimental setup and procedure

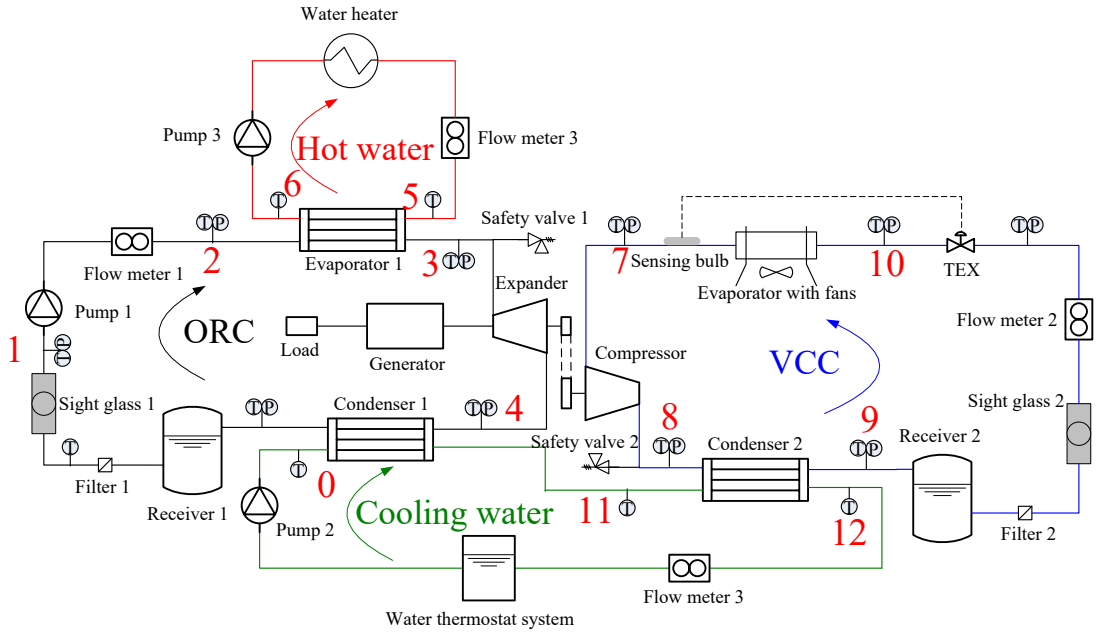

Figure 1. Schematic diagram of ORC-VCC combined system

As schematically shown in Fig.1, a small-scale heat driven refrigeration system that integrates an ORC power plant with a vapour compression refrigerator was designed and constructed using off-the-shelf components.

In the ORC subsystem (the loop with black line in Fig.1), R245fa is used as the working fluid due to its desired thermodynamic properties, low toxicity, low flammability, and low corrosiveness. The ORC subsystem consists of an oil-free scroll expander with a rated power output of 1 kW, an evaporator (a plate heat exchanger), two condensers in parallel (plate type) and a diaphragm working fluid circulation pump.

140 The motor connected to the circulation pump is wired with a variable-frequency
141 invertor, which is used to regulate the flow rate of R245fa. Hot water provided by an
142 18 kW water heater (the red part in Fig.2) is used as the heat source to simulate the
143 cooling jacket water of IC engines. The hot water temperature is controlled by a
144 Proportional-Integral-Derivative (PID) controller, which maintains the water
145 temperature at a desired set point. The hot water is circulated by domestic central
146 heating pump, rated to a maximum flow rate of 3.3 m^3/h.

147 In the VCC subsystem, R134a is used as the refrigerant, which is widely used in
148 various mobile air-conditioning applications. The VCC compressor is connected with
149 the ORC expander via a belt transmission unit, of which the expander-compressor speed
150 ratio can be adjusted by changing pulleys with different sizes. The VCC subsystem
151 consists of an oil-free scroll compressor, a fin-tube evaporator with 3 electrical fans, a
152 thermostatic expansion valve (TEV) and a condenser (a plate heat exchanger). A filter
153 is installed at the receiver tank outlet to remove impurities and a sight glass is installed
154 at the filter outlet to check the state of the refrigerant. A photo of the prototype is shown
155 in Fig.2. The specifications of the main components of the prototype are listed in Table
156 1.

157 The cooling water temperature can be regulated by changing the mixing ratio of
158 cold and hot water steams, varying from 10 to 35 ˚C. As shown in Fig.1, the cooling
159 water firstly flows through the ORC condenser and then the VCC condenser. The VCC
160 evaporator is placed in an enclosure with dimensions of 1.7m×1.4m×0.8m. The fans
161 circulate the air flow inside the enclosure. To prevent heat leakage from the ambient to

the enclosure, it has been insulated using black Nitrile rubber sheets with thickness of 10 mm.

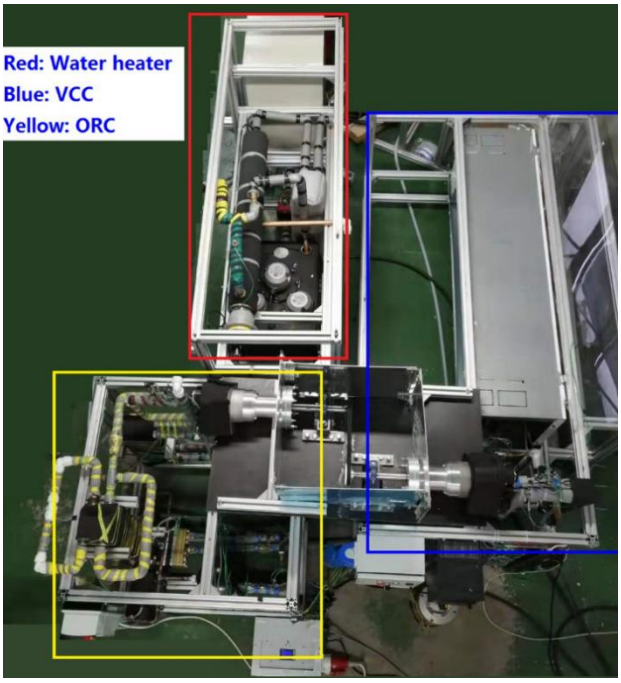

Figure 2. Layout of the ORC-VCC test system

As shown in Fig.1, a number of K-type thermocouples and pressure transducers are installed to measure the temperature and pressure at important test points in the prototype. The specifications of the test equipment are also listed in Tab.1. The test apparatus is equipped with a PCI 16-Bit 1MHz multifunction data acquisition board linked to a computer. According to the measured temperature, pressure and flow rate, the important thermodynamic parameters, including density, enthalpy and entropy at different states, were then determined using Matlab code and the Refprop database [29].

Table 1. Specifications of main components and test equipment

Components	Specifications
Expander	Rated power of 1kW, oil-free, Scroll type, maximum speed of 3600 rpm, volume ratio of 3.5
Condenser-ORC	Two plate type condensers in parallel

Evaporator-ORC	Plate type
Pump	Hydra-Cell seal-less diaphragm pump
Compressor	1 kW oil-free, Scroll, 3600 rpm, volume ratio of 3.5
Condenser-VCC	Plate type
Evaporator-VCC	Fin tube type with 3 fans
Expansion device	Danfoss KAV 10-5, thermostatic expansion valve
Power meter	Measuring uncertainty 0.1 (Frequency) Hz, accuracy of 0.3% F.S. voltage and current
Pressure sensor	Low pressure: PX319-500A5V, accuracy ±0.08% BSL maximum High pressure: PX419-750AV, accuracy ±0.08% BSL maximum
Thermocouple	Type K, 310 Stainless Steel Sheath (-40 to +1100ºC) accuracy ±0.4%t or ±1.5 ºC
Rotational speed sensor	Testo 460, 100~30000rpm, accuracy ±0.1% measured value (100~9999rpm), ±0.02% measured value (10000~30000rpm)
Flow meter of cooling water	Turbine Flow Sensor, 2 L/min~30 L/min, ±3 % of the normal range
Flow meter of refrigerant	Hall effect turbine flow meter, maximum working pressure 10 bar, maximum temperature 125ºC, 0.2-4.5 L/min, accuracy ±1.5% FSD

174

175 Based on the enthalpies calculated by the measured temperature and pressure, the
176 heat transferred in the Evaporator-ORC, Condenser-ORC, Evaporator-VCC and
177 Condenser-VCC can be calculated as the following:

178 $$Q_{eva,ORC} = m_{f,ORC}(h_3 - h_2) \quad (1)$$

179 $$Q_{cond,ORC} = m_{f,ORC}(h_4 - h_1) \quad (2)$$

180 $$Q_{eva,VCC} = m_{f,VCC}(h_7 - h_{10}) \quad (3)$$

$$Q_{cond,VCC} = m_{f,VCC}(h_8 - h_9) \quad (4)$$

The ORC was connected to the VCC by using a belt transmission unit. The mechanical loss through the belt power transmission system is ignored and the compressor power is assumed to be equal to that generated by the expander.

$$W_{com} = W_{exp} \quad (5)$$

As the ORC-VCC is essentially a heat driven refrigeration system, the heat-to-cooling efficiency is defined to evaluate the system performance of the combined system as:

$$\eta_{H-C} = \frac{Q_{eva,VCC}}{Q_{eva,ORC}} = COP_c(\eta_{ORC} + \frac{W_P}{Q_{eva,ORC}}) \quad (6)$$

The expander-compressor speed ratio is defined as the ratio of the expander speed to the compressor speed:

$$SR = \frac{n_{exp}}{n_{com}} \quad (7)$$

3 Results and discussion

The reading of the thermocouples, pressure transducers, and flow meters are recorded using the data acquisition system at a sampling frequency of 0.2 Hz. Both the steady and transient behaviour of the combined ORC-VCC system have been tested.

3.1 Uncertainty analysis

The performance of the system was measured at various inlet temperatures of heat source and sink, when the flow rates of working fluids and cooling water varied. The accuracy of measured parameters listed in Table. 1 were considered with the system error propagation. The Kline and McClintock relationship [33] has been employed to

calculate the total uncertainty of heat-to-cooling efficiency. For example, the temperature of refrigerant at the ORC evaporator inlet and outlet are 18.2±0.07 ˚C and 94.0±0.38 ˚C, respectively. The inlet and outlet pressure are 109.94± 0.09 PSI and 106.01± 0.08 PSI, respectively. The flow meter of the ORC refrigerant , 0.0403±0.0027 kg/s, is also required to calculate the density and mass flow rate of the refrigerant. In this approach, the relative error of heat-to-cooling can be calculated to be around 6.75%.

3.1 Steady state test of ORC-VCC

This section discusses the performance of the ORC-VCC prototype operated under partial load conditions at a steady state. The performance is evaluated based on the characteristics mainly of the VCC cycle, the refrigeration temperature, the cooling capacity and the overall heat-to-cooling efficiency. Due to the large amount of experimental data collected, the effects of different operating parameters have been considered, including the mass flow rate of ORC working fluid and the expander-compressor speed ratio.

3.1.1 Effect of ORC mass flow rate

The heat source temperature remains at 94.6 °C. The mass flow rate of the cooling water is kept constant at 0.173 kg/s. The expander-compressor speed ratio is 1.71, using the pulleys with 28 and 48 teeth at expander and compressor side, respectively. Since the teeth on the pulleys are of the same size, the diameters are proportional to the teeth number. For the vapour compression refrigeration subsystem, the compressor speed is commonly used to control cooling capacity and cooling temperature. In the experimental procedure, the compressor rotation speed is controlled by the expander in

ORC. Therefore, the effect of the ORC mass flow rate on the system performance under different cooling water temperatures and heat source temperature is studied to explore the interactions between ORC and VCC in this section.

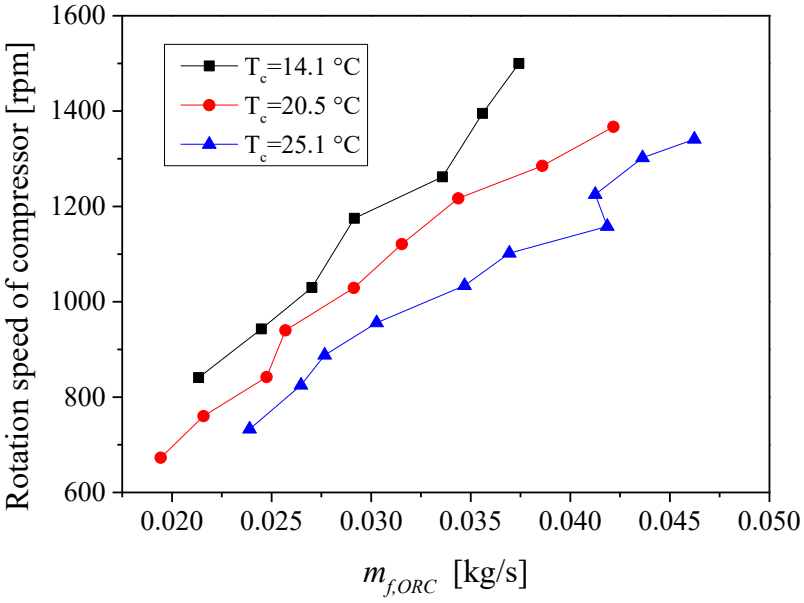

Figure 3. Rotation speed of compressor with respect to variation of ORC mass flow rate under different cooling water temperatures

Figure 3 shows that the compressor rotation speed increases with the rise of the mass flow rate of working fluid in the ORC subsystem ($m_{f,ORC}$). When ORC subsystem is operated at a smaller mass flow rate, the superheat of the working fluid at the expander inlet is relatively higher. As the mass flow rate ($m_{f,ORC}$) increases, the pressure difference across the expander increases but the superheat degree decreases. The maximum pressure difference would appear when the superheat degree becomes 0. If the flow rate keeps increasing further, part of the working fluid can't evaporate in the evaporator, leading to a decrease in its evaporation pressure. In these tests, the working fluid at the expander inlet is kept within the superheated region. Subsequently, when

the mass flow rate $m_{f,ORC}$ was increased by increasing the liquid pump frequency, both the expander intake pressure and the expander rotation speed increase. Since the mass flow rate of the cooling water is kept constant, it is also clear that a lower temperature of cooling water can lead to a higher rotation speed of compressor due to the lower condensation pressure as expected.

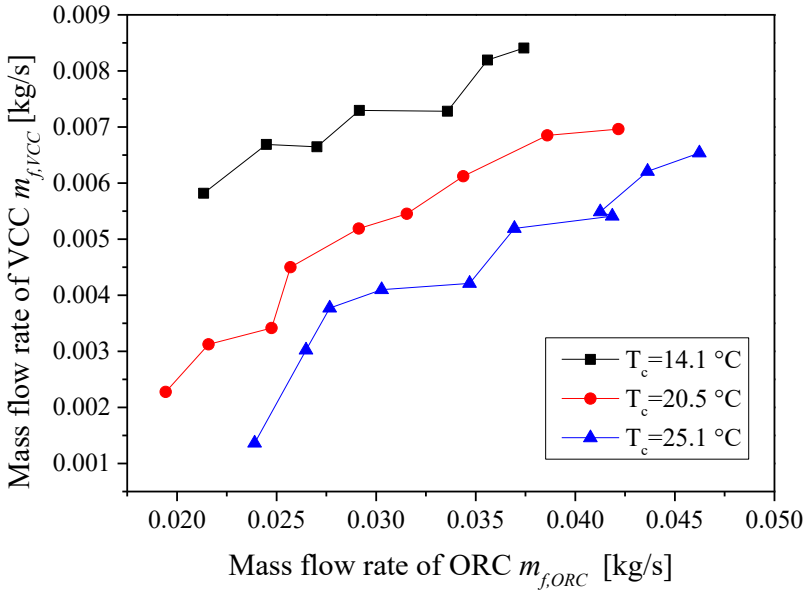

Figure 4. Mass flow rate of R134a in the VCC with respect to the mass flow rate of R245fa of ORC

It is observed from Fig.4 that the mass flow rate of the refrigerant R134a ($m_{f,VCC}$) is proportional to the flow rate of the ORC working fluid R245fa. As mentioned above, the compressor speed increases with the increase of $m_{f,ORC}$. In the tested ORC-VCC prototype, the scroll compressor is a positive displacement compressor and the expansion valve is a thermostatic expansion valve (TEV). It is known that the cooling capacity and the refrigeration temperature of a VCC system are normally controlled by regulating flow rate of the refrigerant and the pressure difference across TEV by

adjusting the compressor rotation speed and spring pressure of TEV. For a constant spring pressure inside TEV, more refrigerant will be allowed to pass since the volumetric flow rate increases as the compressor's rotation speed increases. For a given compressor rotation speed, a lower cooling water temperature tends to open the TEV further due to a larger pressure difference resulting from a lower condensation pressure. For the ORC subsystem, the expander will speed up by lowering the cooling water temperature, increasing the compressor rotation speed. Therefore, $m_{f,VCC}$ increases as expected, which can be attributed to the increasing compressor speed and the enlarged TEV opening.

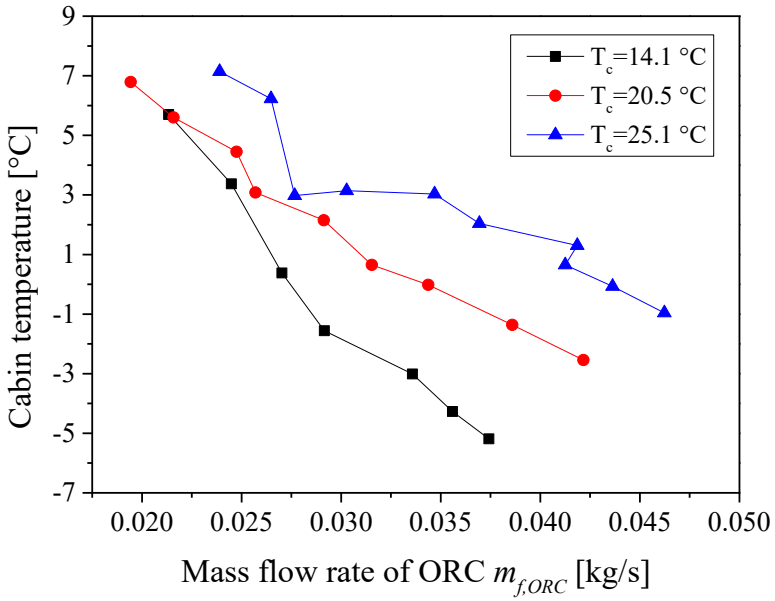

Figure 5. Effect of the ORC mass flow rate $m_{f,ORC}$ on the temperature inside the enclosure under different cooling water temperatures

Figure 5 presents the variation of inside temperature under different cooling water temperatures. In the tests, the cooling water firstly flows into the VCC condenser and then the ORC condenser. Its original temperature will affect both ORC and VCC

significantly. From the perspective of ORC subsystem, the pressure difference across the expander will be reduced if the condensation temperature increases for a given evaporation pressure. As a result, the pressure difference across the compressor also decreases for a given speed ratio since it is driven by the ORC expander. Meanwhile, the VCC subsystem's evaporation pressure P_7 decreases since the VCC compressor outlet pressure P_8 decreases with the decrease of the cooling water temperature. That is why the evaporation temperature in the VCC subsystem decreases with the decrease of condensation temperature, and the colling load enclosure can reach a lower temperature. The temperature inside the enclosure will be affected by other external factors (the ambient temperature outside, the insulation material and thickness etc.). The temperature can be maintained as low as -5.6 °C in all the tested conditions when the cooling water temperature is 14.1 °C.

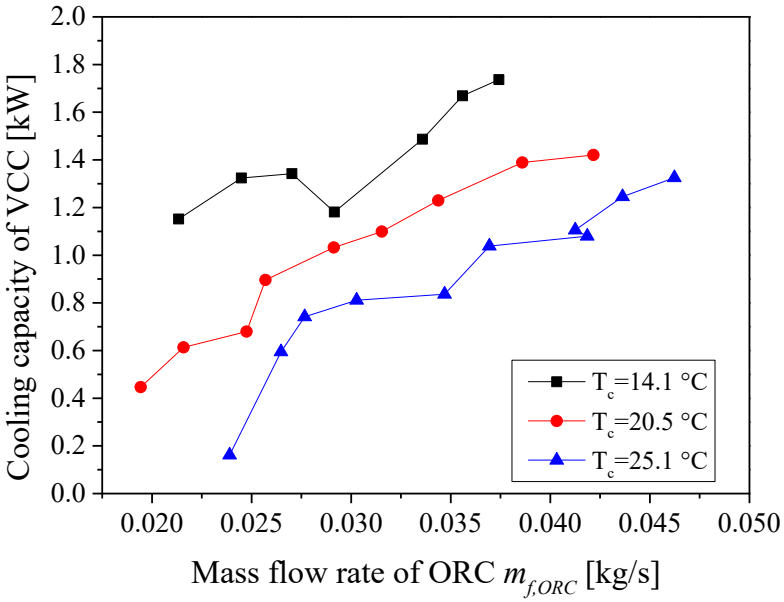

Figure 6. Effects of the ORC mass flow rate on the cooling capacity under different cooling water temperatures

Figure 6 shows the variation of the cooling capacity against $m_{f,ORC}$ under different cooling water temperatures. When the other control parameters remain unchanged, the cooling capacity will be enhanced by increasing the compressor speed due to the increased flow rate of refrigerant in the VCC and the decreased condensation temperature. This is the reason why the cooling capacity increases with the mass flow rate of working fluid in the ORC subsystem in Fig. 6. Moreover, the variation of cooling water temperature affects both ORC and VCC subsystems. For a lower condensation temperature, at the ORC side, the reduction of the condensation temperature would lead to a larger enthalpy drop of the refrigerant across the expander, leading to a higher power generation. At the VCC side, a higher power transmitted from ORC by the belt transmission unit would increase the cooling capacity in the VCC system. The maximum cooling capacity reaches 1.74 kW under all the test conditions. A sudden drop is shown at the ORC flow rate of 0.028 kg/s. This can be attributed to the fact that the working fluid at the VCC evaporator turns into a two-phase mixture according to the measured temperature and pressure. As a result, some of the refrigerant doesn't evaporate, so less heat is absorbed by the refrigerant.

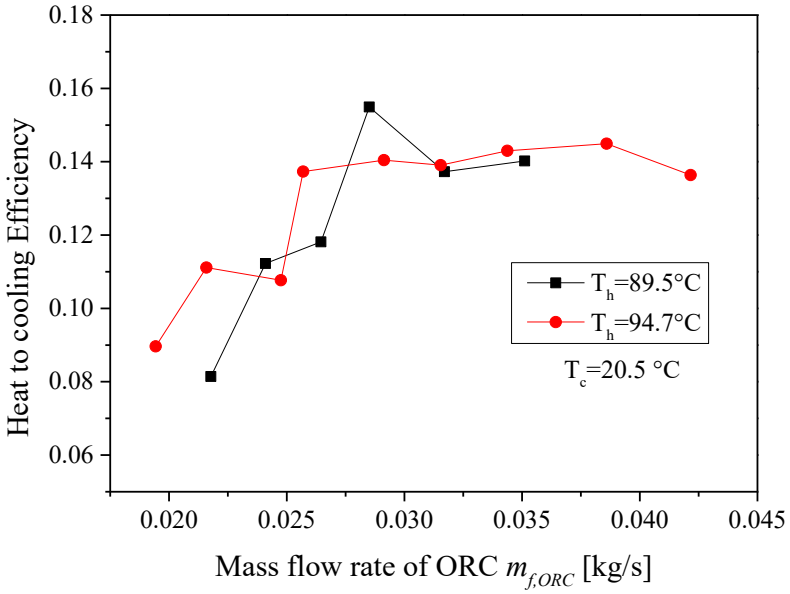

Figure 7. Comparison of heat-to-cooling efficiency between different heat source temperatures

Since this prototype is essentially a heat driven refrigeration system, a heat-to-cooling efficiency is used to evaluate the ability of cooling capacity by consuming thermal energy. Fig.7 shows the comparison of heat-to-cooling efficiency under the same cooling water temperature (T_c=20.5 °C), and two different heat source (i.e., hot water) temperatures T_h. It is indicated that the heat-to-cooling efficiency of the ORC-VCC show a similar variation trend with different heat source temperatures, both increasing firstly before reaching a plateau or slight downward trend. According to Eq. (6), the heat-to-cooling efficiency is proportional to the ORC thermal efficiency and COP_c of VCC. From our previous study on a separate ORC experiment, the thermal efficiency increases firstly and then decreases as the $m_{f,ORC}$ increases, and the peak appears when the superheat degree is around 0. These results agree well with those in Miao [30] and Kosmadakis's [31] study. As shown in Fig.3, the compressor speed

increases as $m_{f,ORC}$ increases. The COP_c decreases as the pressure ratio reduces, which is proportional to the compressor rotation speed, as explained in Mateu-Royo's research [22]. As a result, the combined effect results in the variation trend of heat-to-cooling efficiency as shown in Fig.7, increasing firstly and then decreasing.

3.1.2 The effect of speed ratio between expander and compressor

From the analysis above, it is found that the load significantly affects the power output, the overall efficiency of expander and generator set of the ORC subsystem. Our original design connects the expander and the compressor using a directly driven shaft, leading to exactly the same rotational speed and torque. However, based on previous calculation results [29], when the ORC and VCC subsystems are operated separately, it is found that the pressure drop across the expander is different from that across the expander when they are operated under the optimal conditions for a given heat source and heat sink conditions. In other words, sharing a common shaft between expander and compressor does not allow that the ORC and VCC to operate under their own optimal conditions simultaneously because their torque profiles mismatch with each other. Therefore, a belt transmission unit is used to study the effect of the speed ratio of expander-compressor on the operation and the system performance. Four pairs of pulleys are used in this test, of which the teeth ratios are 28/48, 32/44, 36/44 and 32/36, respectively. Since the size of teeth are exactly the same of these pulleys, the correspondingly speed ratios of expander-compressor are 1.71 (48/28), 1.38 (44/32), 1.22(44/36) and 1.13 (36/32), respectively. The temperatures of heat source and cooling water are approximately 367K and 293K, respectively.

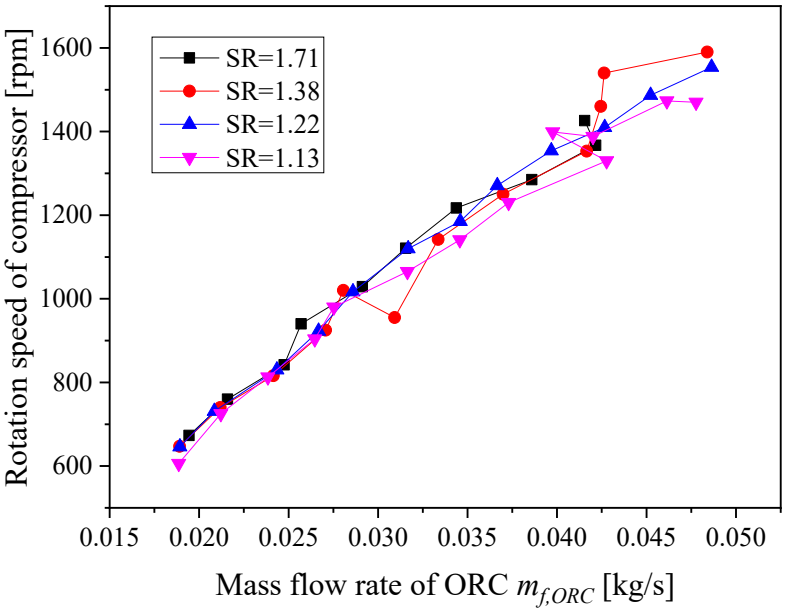

Figure 8. Comparison of compressor rotation speed between different speed ratios

The results in Fig.8 indicate the compressor rotation speed increases proportionally with the increase of $m_{f,ORC}$, which seems to be independent from the speed ratio. From the perspective of system operation, the VCC subsystem can be regarded as a variable load of the ORC subsystem. While the ORC subsystem acts as the power source of the VCC subsystem. The variation of load and speed in the ORC subsystem will cause the change of the VCC subsystem's operating conditions. At the same time, the VCC subsystem will feedback such changes to the ORC subsystem through the belt since the compression ratio and speed in the VCC subsystem are dependent on each other.

For the ORC subsystem, the load has significant impact on the power generation, including the rotation speed and the torque output. The output torque of the expander is closely related to the pressure drop across the expander in the ORC subsystem. During this test, the ORC subsystem's fluid pump is operated at a given frequency. For

the VCC subsystem, the rotational speed affects the mass flow rate of the refrigerant significantly, and the torque input is closely related to the compression ratio. As shown in Eq. (5), the power consumed by the compressor is delivered by the expander. Furthermore, the speed at the circumference of these two pulleys is equal to each other as there is no slippage. As a result, the rotation speeds of both ORC and VCC subsystems present the same variation trend, increasing as the mass flow rate of working fluid of the ORC subsystem increases.

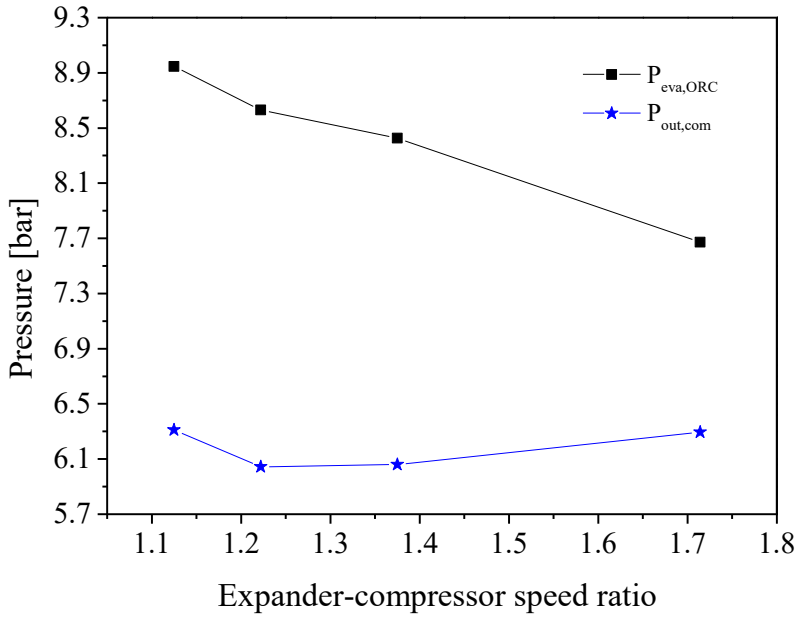

Figure 9. Pressures at the expander inlet and compressor outlet with different speed ratios

Therefore, when the pulley pairs with higher expander to compressor speed ratios are used, the expander rotational speed will be increased for a given $m_{f,ORC}$. This can be attributed to the reduced torque output and expansion ratio since the measured evaporation pressure $P_{eva,ORC}$ is decreased, as shown in Fig.9.

For the VCC subsystem, the increased expander rotational speed would lead to an

upward trend of the compressor rotation speed. However, the radius of the pulley connected to the compressor is also larger, which would restrain the increase of the compressor rotation speed. Leading to the minor difference of compressor rotational speed while using pulley pairs with different speed ratios.

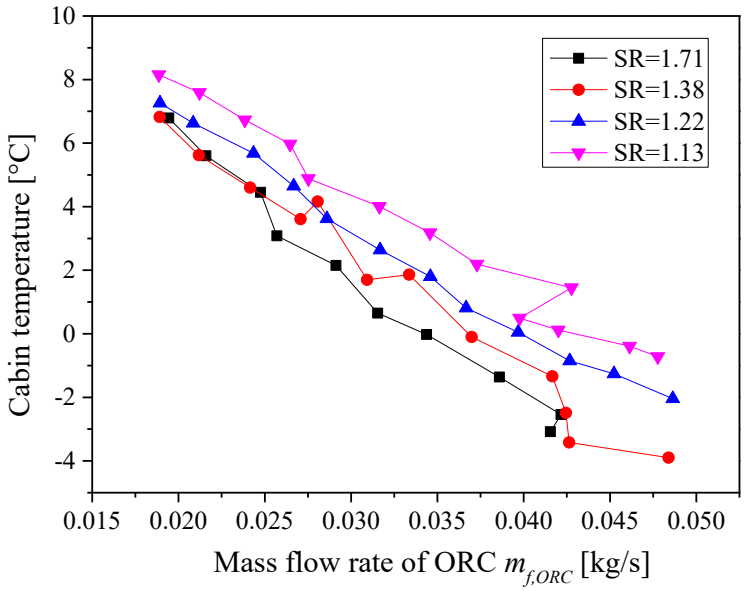

Figure 10. Comparison of temperature inside the enclosure between different speed ratios

For the combined ORC-VCC cycles, there are two important parameters for evaluating the system performance, cooling temperature and cooling capacity. The temperature inside the enclosure, which is closely related to evaporation temperature of the VCC subsystem, is a target temperature according to real applications. In the VCC subsystem, the evaporation temperature is controlled by adjusting the rotation speed of the compressor. It is noted from Fig.10 that a lower temperature can be achieved by increasing $m_{f,ORC}$. This is due to the fact that the increasing $m_{f,ORC}$ will increase the rotation speed, which results in higher $m_{f,VCC}$ and pressure drop across the TEV,

leading to a lower evaporation temperature as shown in Fig.10. The lowest temperature in the tests is -3.9 °C when the speed ratio is 1.38.

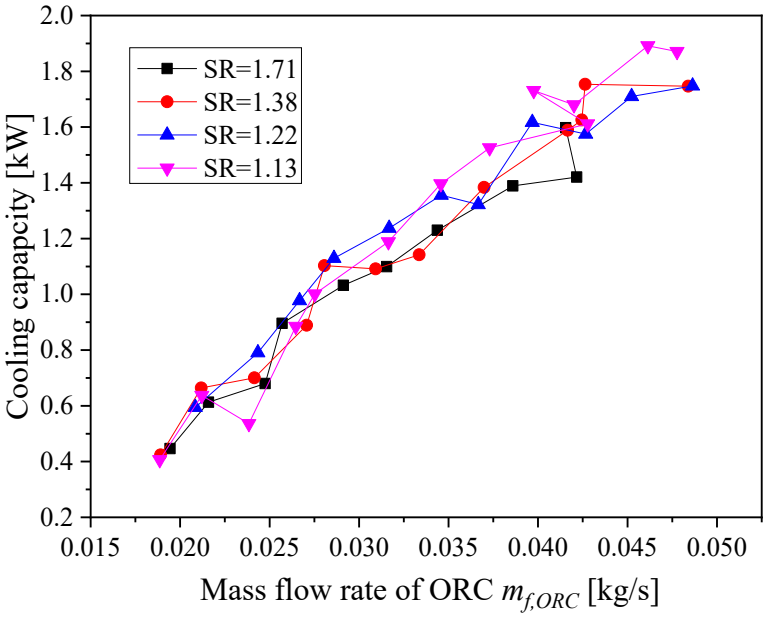

Figure 11. Cooling capacity of the system when the speed ratio varies

Figure 11 indicates that the cooling capacity increases with the increase of $m_{f,ORC}$. The cooling capacity is affected by both $m_{f,VCC}$ and the temperature lift of the refrigerant. The reason why the cooling capacity increases with $m_{f,ORC}$ has been explained in Fig.6. It is also noted that the cooling capacity is a bit smaller when the system is operated with higher speed ratios, although the difference is insignificant. From the analysis above it can be found that a lower temperature can be realised inside the enclosure when the system operates with a higher expander-compressor speed ratio (shown in Fig.7). In theory, the opening of TEV would become smaller to achieve a higher pressure difference for a given compressor rotation speed, which will result in a smaller $m_{f,VCC}$, leading to a smaller cooling capacity in the VCC subsystem.

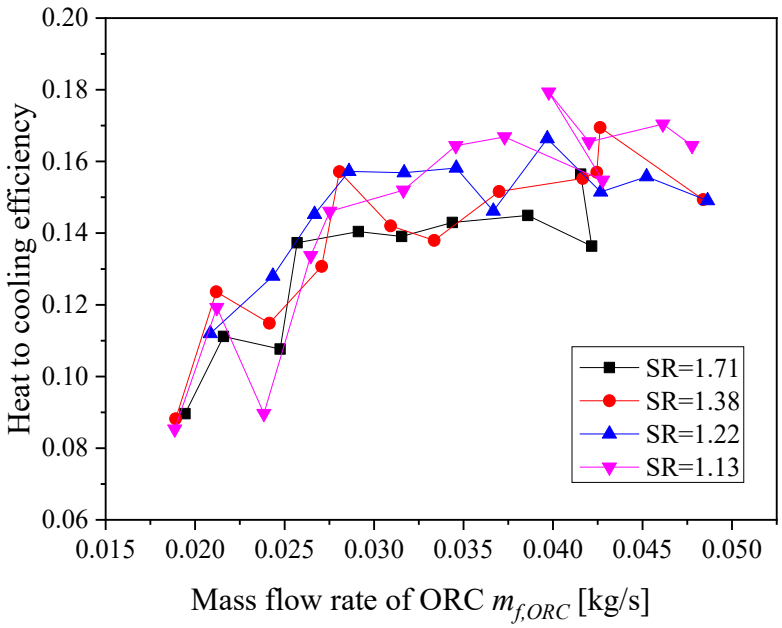

Figure 12. Comparison of heat-to-cooling efficiency between different speed ratios

Figure 12 presents the comparison of heat-to-cooling efficiency when the prototype operates with different speed ratios. Although the heat-to-cooling efficiencies fluctuate, the curves with different speed ratios all show a similar trend, increasing sharply firstly and then gradually flattening. The maximum heat-to-cooling efficiency is about 0.18 in these tests. When $m_{f,ORC}$ was increased by increasing the fluid pump frequency, more power is available to drive the compressor. During this process, the mass flow rate $m_{f,VCC}$ is controlled by the TEV through the feedback of the sensing bulb located at the evaporator outlet. Both the evaporation temperature and condensation temperature (essentially differential pressure across the TEV) can affect the opening of the TEV, and thus affects the amount of fluid available for cooling. As illustrated, both the ORC evaporator and the VCC evaporator absorb more heat from hot water and ambient air, respectively. The different growth of the heat transfer leads to the variation of heat-to-

cooling efficiency as shown in Fig.12. Although the test result fluctuate, we can still tell from the curves that the heat-to-cooling efficiency is lower when the system is operated with a higher expander-compressor speed ratio, which can be attributed to the lower cooling capacity as mentioned previously.

3.2 **Transient state of ORC-VCC**

Due to the direct mechanical coupling between two subsystems, when one subsystem experiences operational change, unsurprisingly it can result in a change to the other. In order to ensure the system can quickly react to regulation and become stable, it is important to investigate the transient response of the whole system. In this section, the temperature and mass flow rate of the cooling water are maintained at 20.5 °C and 0.173 kg/s during the test, respectively. The temperature of the hot water was kept constant at 368K.

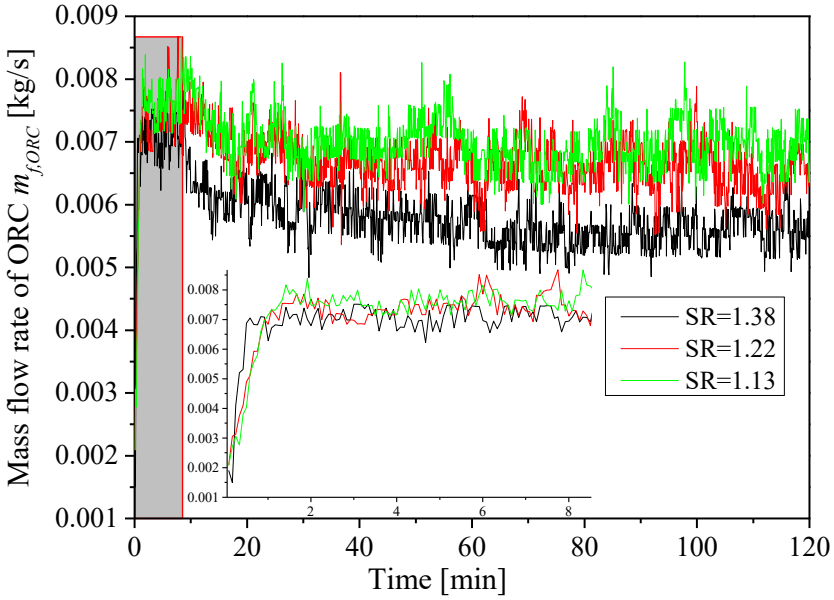

Figure 13. Transient responses of ORC mass flow rate to a sudden increase of ORC circulation pump under different expander-compressor speed ratios

The initial temperatures inside the enclosure are 7.4 °C, 5.7 °C and 6.8 °C respectively. The tested speed ratios of the expander-compressor are SR=1.375, SR=1.222 and SR=1.125, respectively. The hot water (heat source) temperature is approximately 95 °C and the cold water (heat sink) is about 20.5 °C. The ORC circulation pump was initially operated at 10 Hz and it was suddenly increased to 16 Hz. Fig.13 shows how the pump reacts to a change in the mass flow rate and the response time until the flow rate stabilises. It can be seen in Fig.13 (zooming in part) that the mass flow rate of ORC rises to a relatively stable value in less than 2 minutes. During the entire process of experiment, the flow rate fluctuates around an average value. The fluctuation can be attributed to the working principle of the diaphragm pump, which is similar to the piston pump.

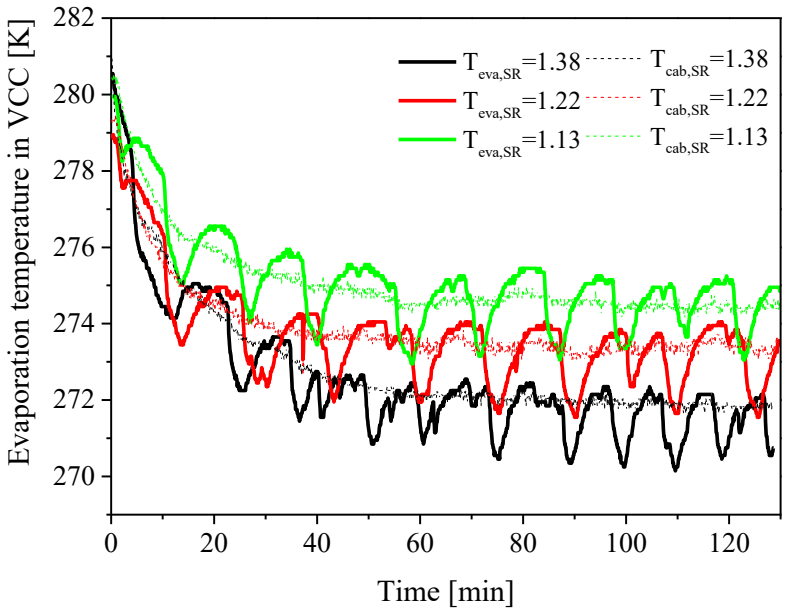

Figure 14. Transient responses of VCC evaporation temperature and the temperature

453 inside the enclosure to a sudden increase of ORC working fluid pump under different
454 expander-compressor speed ratios
455
456 Fig.14 presents the dynamic behaviour in terms of the transient responses of the
457 VCC evaporation temperature and the temperature inside the cooling enclosure to a
458 sudden increase of the frequency of the working fluid pump of the ORC subsystem.
459 The results indicate that the evaporation temperature of the VCC oscillates periodically,
460 the TEV maintains the swing in a range of ±1 K around the set value. Generally, the
461 variation trend is decreasing although their peak and trough values oscillate, and finally
462 become stable. In this system, a bulb sensing element is located at the evaporator outlet
463 pipe to control the opening degree of the TEV, which determines the flow area of the
464 TEV according to the feedback from the bulb. The fluctuation of the evaporation
465 temperature results from the variation of the TEV opening degree. The larger the
466 opening, the higher the mass flow rate.
467 It is well known that when the heat absorbed from the enclosure and the cooling
468 generated in the evaporator achieve balance, the temperature inside the enclosure will
469 become constant. From Fig.14, it can be noticed that the enclosure temperature (dot
470 line) starts to decrease since the ORC pump frequency rises which steadies out after a
471 period of time. These periods, from the triggering of the working fluid pump frequency
472 to the balanced state, are different. When the system was operated with a higher speed
473 ratio, the enclosure temperature can be maintained at a lower value as the temperature
474 becomes stable. The sustained oscillatory behaviour of the evaporation temperature can
475 be improved by using an electronic expansion valve (EEV), which can perform better

since it can achieve a precise regulation for optimal control of mass flow rate even under off-design condition.

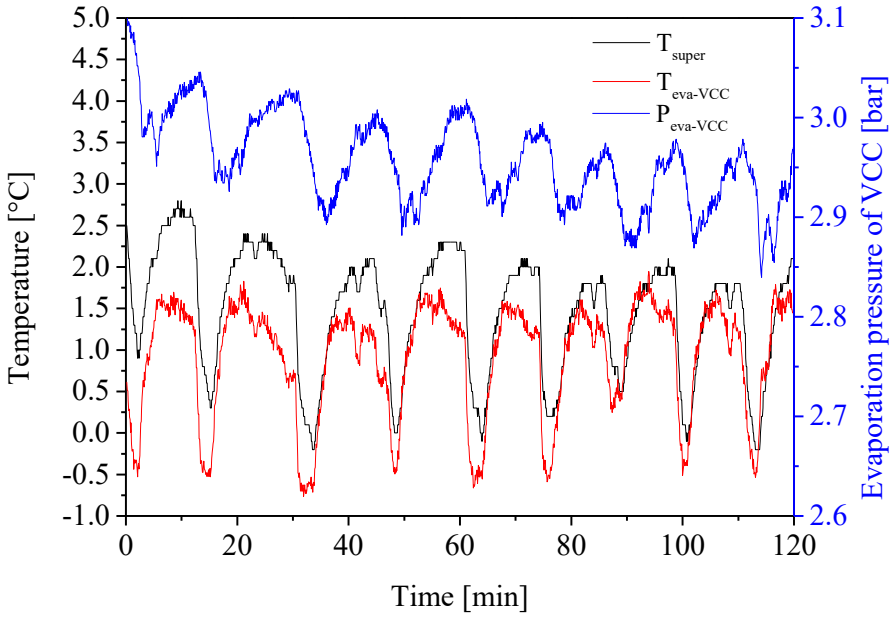

Figure 15. Variation of evaporation temperature, pressure and the corresponding superheat degree with response to TEV characteristics, SR=1.12

Interesting results can be found in Fig.15, which records the evaporation temperature $T_{eva,\,VCC}$, evaporation pressure $P_{eva,VCC}$ and superheat degree T_{super} of the VCC when the combined cycle is running under a steady state. Thermal expansion valve (TEV) is typically a linear controller operating simply in response to a change in evaporator superheating. The sensing bulb possess a proportional feedback action control mechanism to keep evaporator superheating at a constant value. When the expansion valve remains unchanged, the differential pressure between the bulb and the evaporation tube equals the spring force. Once the superheating is higher than the set value, the balance will be broken and the opening becomes larger. That is why the

491 evaporator pressure shows a typical oscillation response that was obtained by adjusting
492 the static superheat setting. Fig.15 also shows that the superheating of the tested
493 prototype varies from 0.75 °C to 3.25 °C under oscillation. The superheating grows as
494 soon as the opening of TEV decreases. When the superheating is over its set value of
495 2.5 °C, the opening of TEV will increase. The superheating appears to have a flat region
496 and it can be maintained around the peak value for a longer time. This could be
497 attributed to the TEV characteristics. The TEV should be superheated vapour before
498 flowing into the compressor, avoiding the risk of causing damage to the compressor. As
499 no more energy is available to evaporate the liquid refrigerant inside the evaporator, the
500 pressure difference between the sensing bulb and the evaporation tube deceases. As a
501 respond to this change, the opening of TEV will decrease as soon as the superheating
502 reaches the trough value, which is closely related to the spring force inside. The
503 behaviour of the evaporation temperature is more revealing. The timings of temperature
504 variation and that of pressure variation are different. There is a delay in the response of
505 the TEV due to friction and flow experienced by the valve. The performance can be
506 improved by replacing the TEV by Electronic expansion valve (EEV).

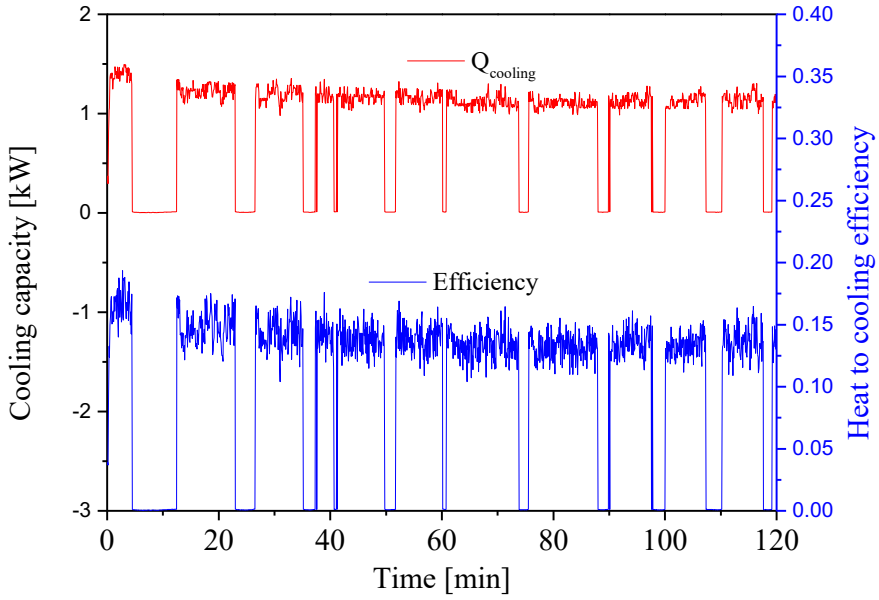

Figure 16. Cooling capacity and heat-to-cooling efficiency during transient state

The result shown in Fig.15 and Fig.16 are measured when the heat source temperature and cold source temperature are 95 °C and 19.7 °C respectively. The speed ratio of expander-compressor is 1.125.

Figure 16 shows the variation of cooling capacity and its heat-to-cooling efficiency of the combined cycle, both of which appear to present a similar trend. In general, the cooling capacity variation presents a peak value and trough value during the test procedure. The peak value is about 1.4 kW and the trough is 0 kW. Such a typical 'hunting' response was obtained by adjusting the static superheat setting by balancing the differential pressure across TEV. The variation trend of cooling capacity could be attributed to the TEV characteristics because the refrigerant flow rate is the direct output of the TEV. In general, the cooling capacity has 'flat' regions at the peak and the trough of the oscillations. The trough flat region of 0 kW indicates that the TEV is shut off and

there is no refrigerant R134a flowing through the TEV. Generally speaking, the flat regions at the peak is larger than that at the valley. Meanwhile, the heat-to-cooling efficiency of the overall combined system at the peak is around 0.15. The prototype can have a higher heat-to-cooling efficiency since this is the part load condition of both the ORC and VCC.

4 Conclusions

In this study, a lab-scale heat driven ORC-VCC refrigerator was constructed and tested under a wide range of operating conditions. The system aims to generate cooling effects by recovering the low-temperature heat contained in the cooling-jacket water. Several remarks can be summarised as follows:

(1) The expander-compressor speed ratio has minor effect on the heat-to-cooling efficiency of the whole system.

(2) A lower enclosure temperature can be achieved when a higher expander-compressor speed ratio is adopted, while its cooling capacity is a bit smaller.

(3) The measured minimum enclosure temperature and maximum heat-to-cooling efficiency is -5.6 °C and 0.18, respectively, under partial load conditions.

(4) The fluctuation of the VCC refrigeration subsystem is mainly caused by opening of the TEV.

In a summary, this research has demonstrated the concept of the ORC-VCC combined cycle for small scale thermally driven refrigeration applications. Further investigation under the design condition will be carried out to optimize system performance in the next steps. The transient performance can be improved by replacing the TEV by EEV.

Acknowledgment

The authors like to acknowledge EPSRC (EP/N020472/1, EP/N005228/1, and EP/R003122/1) in the United Kingdom for the financial support to this research.

Reference

[1] IEA (2020), Global CO_2 emissions in 2019, IEA, Paris https://www.iea.org/articles/global-co2-emissions-in-2019.

[2] Edenhofer O, Pichs-Madruga R, Sokona Y, et al. Contribution of Working Group III to the Fifth Assessment Report of the Intergovernmental Panel on Climate Change. Climate Change, 2014, 1-11.

[3] Zhu S, Zhang K, Deng K. A review of waste heat recovery from the marine engine with highly efficient bottoming power cycles. Renewable and Sustainable Energy Reviews, 2020, 120: 109611.

[4] Shu G, Liang Y, Wei H, et al. A review of waste heat recovery on two-stroke IC engine aboard ships [J]. Renewable and Sustainable Energy Reviews, 2013, 19(1):385-401.

[5] Li B, Wang S, Wang K, et al. Thermo-economic analysis of a combined cooling, heating and power system based on carbon dioxide power cycle and absorption chiller for waste heat recovery of gas turbine[J]. Energy Conversion and Management, 2020, 224: 113372.

[6] Yang S, Deng C, Liu Z. Optimal design and analysis of a cascade $LiBr/H_2O$ absorption refrigeration/transcritical CO_2 process for low-grade waste heat recovery[J]. Energy Conversion and Management, 2019, 192: 232-242.

[7] Pan Q, Peng J, Wang R. Application analysis of adsorption refrigeration system for solar and data center waste heat utilization[J]. Energy Conversion and Management, 2020: 113564.

573 [8] Karellas S, Braimakis K. Energy–exergy analysis and economic investigation of a
574 cogeneration and trigeneration ORC–VCC hybrid system utilizing biomass fuel and
575 solar power[J]. Energy conversion and management, 2016, 107: 103-113.
576 [9] Liang Y, Shu G, Tian H, et al. Analysis of an electricity-cooling cogeneration system
577 based on RC-ARS combined cycle aboard ship [J]. Energy conversion and management,
578 2013, 1;76:1053-60.
579 [10] Liang Y, Shu G, Tian H, et al. Theoretical analysis of a novel electricity-cooling
580 cogeneration system (ECCS) based on cascade use of waste heat of marine engine[J].
581 Energy Conversion and Management, 2014, 85: 888-894.
582 [11] Liang Y, Shu G, Tian H, Sun Z. Investigation of a cascade waste heat recovery
583 system based on coupling of steam Rankine cycle and NH_3-H_2O absorption
584 refrigeration cycle [J]. Energy conversion and management, 2018 166: 607-703
585 [12] Nikbakhti R, Wang X, Hussein AK, et al. Absorption cooling systems–Review of
586 various techniques for energy performance enhancement. Alexandria Engineering
587 Journal, 2020, 59.2: 707-738.
588 [13] Prigmore, D and Barber R. Cooling with the sun's heat Design considerations and
589 test data for a Rankine Cycle prototype. Solar Energy, 1975,17(3), 185-192.
590 [14] Wang H, Peterson R, Harada K, et al. Performance of a combined organic Rankine
591 cycle and vapor compression cycle for heat activated cooling. Energy, 2011, 36(1),
592 pp.447-458.
593 [15] Wang H, Peterson R and Herron T. Design study of configurations on system COP
594 for a combined ORC (organic Rankine cycle) and VCC (vapor compression
595 cycle). Energy, 2011, 36(8), pp.4809-4820.
596 [16] Wali E, Working fluids for solar, rankine-cycle cooling systems. Energy, 1980,
597 5(7), pp.631-639.
598 [17] Wali E, Optimum working fluids for solar powered Rankine cycle cooling of
599 buildings. Solar Energy, 1980, 25(3), pp.235-241.
600 [18] Liang Y, Yu Z, Li W. A waste heat driven cooling system based on combined
601 organic Rankine and vapour compression refrigeration cycles. Applied Sciences. 2019
602 Jan;9(20):4242.

603 [19] Kutlu, Cagri, et al. A study on heat storage sizing and flow control for a domestic
604 scale solar-powered organic Rankine cycle-vapour compression refrigeration
605 system. Renewable Energy, 2019, 143: 301-312.
606 [20] Aphornratana S, Sriveerakul T. Analysis of a combined Rankine–vapour
607 compression refrigeration cycle[J]. Energy Conversion and management, 2010, 51(12):
608 2557-2564.
609 [21] Bu X, Wang L, Li H. Performance analysis and working fluid selection for
610 geothermal energy-powered organic Rankine-vapor compression air conditioning[J].
611 Geothermal Energy, 2013, 1(1): 2.
612 [22] Bu X B, Li H S, Wang L B. Performance analysis and working fluids selection of
613 solar powered organic Rankine-vapor compression ice maker[J]. Solar Energy, 2013,
614 95: 271-278.
615 [23] Bu X, Wang L, Li H. Working fluids selection for fishing boats waste heat powered
616 organic Rankine-vapor compression ice maker[J]. Heat and mass transfer, 2014, 50(10):
617 1479-1485.
618 [24] Bao J, Zhang L, Song C, et al. Comparative study of combined organic Rankine
619 cycle and vapor compression cycle for refrigeration: Single fluid or dual fluid?[J].
620 Sustainable Energy Technologies and Assessments, 2020, 37: 100595.
621 [25] Demierre J, Henchoz S, Favrat D. Prototype of a thermally driven heat pump based
622 on integrated Organic Rankine Cycles (ORC) [J]. Energy, 2012, 41(1)10-17.
623 [26] Demierre J, Favrat D, Schiffmann, et al. Experimental investigation of a Thermally
624 Driven Heat Pump based on a double Organic Rankine Cycle and an oil-free
625 Compressor-Turbine Unit [J]. International Journal of Refrigeration, 2014, 44: 91-100.
626 [27] Wan X, Cai L, Yan J, et al., Power management strategy for a parallel hybrid-power
627 gas engine heat pump system [J]. Applied Thermal Engineering, 2017, 110: 234-43.
628 [28] Shang S, Li X, Wu W, et al., Energy-saving analysis of a hybrid power-driven heat
629 pump system [J]. Applied Thermal Engineering, 2017, 123:1050-9.
630 [29] Liang Y, Al-Tameemi M, Yu Z. Investigation of a gas-fuelled water heater based
631 on combined power and heat pump cycles [J]. Applied Energy, 2018, 212: 1476-1488
632 [30] Miao Z, Xu J, Zhang K. Experimental and modeling investigation of an organic

633 Rankine cycle system based on the scroll expander. Energy, 2017, 134, 35-49.
634 [31] Kosmadakis G, Mousmoulis G, Manolakos D, et al. Development of open-drive
635 scroll expander for an Organic Rankine Cycle (ORC) engine and first test
636 results. Energy Procedia, 2017, 129, 371-378.
637 [32] Mateu-Royo C, Navarro-Esbrí J, Mota-Babiloni A, et al. Experimental exergy and
638 energy analysis of a novel high-temperature heat pump with scroll compressor for waste
639 heat recovery. Applied Energy, 2019, 253, 113504.[33] Mcclintock F. Describing
640 uncertainties in single-sample experiments. Mechanical Engineering. 1953;75(1):3-8.
641